Applied Surface Science 645 (2024) 158824

Contents lists available at ScienceDirect

Applied Surface Science

journal homepage: www.elsevier.com/locate/apsusc

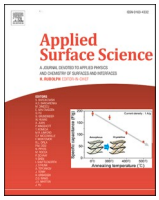

Full Length Article

Polymerization mechanisms of hexamethyldisiloxane in low-pressure plasmas involving complex geometries

Paula Navascués [a,*], Martina Buchtelová [b], Lenka Zajícková [b,c], Patrick Rupper [a], Dirk Hegemann [a]

[a] Laboratory for Advanced Fibers, Empa, Swiss Federal Laboratories for Materials Science and Technology, Lerchenfeldstrasse 5, 9014 St. Gallen, Switzerland
[b] Central European Institute of Technology - CEITEC, Brno University of Technology, Purkyňova 123, 612 00 Brno, Czech Republic
[c] Department of Condensed Matter Physics, Faculty of Science, Masaryk University, Kotlářská 2, 611 37 Brno, Czech Republic

ARTICLE INFO

Keywords:
Plasma polymerization
HMDSO
ATR-FTIR
Surface oxidation

ABSTRACT

Hexamethyldisiloxane (HMDSO) low-pressure plasmas are known for their versatility in the deposition of plasma polymer films (PPFs) with different properties and applications. Although they have been studied for decades, the reaction mechanisms of plasma polymer formation leave open questions, particularly when deposition on 3D materials with complex geometries such as cavities and undercuts is considered. In the present study, two configurations named "cavity" and "undercut" have been selected to study the influence of diffusion of film-forming species and surface reactivity in HMDSO plasmas without and with O_2 admixture. A varying spatial chemical composition of the plasma polymer deposit along the penetration depth of the studied configurations indicates different sticking probabilities of the film-forming species. Furthermore, although ion-induced effects are usually only considered for direct plasma exposure, the obtained results and additional etching experiments reveal that the contribution of high-energy particles might still be considered underneath small openings. Finally, the relevance of oxidizing chemical reactions at the surface inside the configurations is clarified when O_2 is added to the plasma.

1. Introduction

Plasma polymerization stands out as an ideal technique to deposit polymers at the nanoscale in a homogeneous and controlled manner [1–3]. In particular, plasma enhanced chemical vapor deposition (PECVD) using hexamethyldisiloxane (HMDSO) as a monomer can be carried out at low pressure and room temperature, that is, at mild conditions able to cover sensitive substrates such as textiles or thermoplastic polymers [4]. Typically, at least at the laboratory scale, PECVD processes have been designed to work with plane substrates: one usually refers to thin films as a nanoscale-thick layer homogeneously deposited on a flat substrate. The reasons can be easily understood: on the one hand, thinking in two dimensions (2D) simplifies the coating task; on the other hand, the PECVD technology has been traditionally developed parallel to the requirements of the semiconductor industry for microelectronics applications and, therefore, working with large diameter, flat materials [5]. Nevertheless, the more-than-Moore approach reached in the semiconductor industry actually demands the fabrication of complex 3D nanostructures such as Gate-All-Around FET (GAA FET) transistors [6]. Moreover, novel advanced applications such as those in biomaterials have new requirements, for example, using 3D materials (e.g., scaffolds or complex implants) as substrates [7,8]. This fact opens several questions: how are the plasma polymerization mechanisms affected by these complex geometries? How might the chemistry of the deposited polymers be altered? Zajícková and coworkers recently published a study focusing on these questions using cyclopropylamine as a monomer in a radio-frequency (RF) capacitively coupled plasma (CCP) reactor at low pressure [7]. Combining modeling and experimental data, the authors observed the non-uniform chemistry of the coating along substrates such as hydroxyapatite scaffolds or nanofibrous mats. They discussed the results regarding film-forming species with different values of their sticking coefficient, a factor defined between 0 and 1 (1 meaning that the film-forming species directly stick when they reach the surface [9]).

Following a macroscopic kinetics approach for PECVD, processes taking place in the gas phase can be distinguished from those taking

* Corresponding author.
E-mail address: paula.denavascues@empa.ch (P. Navascués).

https://doi.org/10.1016/j.apsusc.2023.158824
Received 30 June 2023; Received in revised form 10 October 2023; Accepted 31 October 2023
Available online 3 November 2023

place on the surface. For the plasma polymerization of the HMDSO molecule ($(CH_3)_3$-Si-O-Si-$(CH_3)_3$), it is proposed that the potentially film-forming species produced in the gas phase are mainly $(CH_3)_2$-Si-O$^{\cdot}$ and $(CH_3)_2$-Si-$^{\cdot}$ biradicals [4]. For a parallel-plate reactor configuration, where flat substrates are placed on the electrodes, it was observed that mainly the former, O-containing radical constitutes the film growth due to its higher reactivity. Likewise, abstracted –CH fragments have low reactivities and tend to form stable volatile products [10]. When O_2 is added to the plasma, however, the $(CH_3)_2$-Si-$^{\cdot}$ fragment might get oxidized in the gas phase or close to the surface, thus also contributing to film growth. These film-forming species reach the substrate, diffuse along them, and get deposited. Note that for low-pressure conditions, the flow of the film-forming species is considered to be laminar, and, therefore, diffusion is the main mechanism. Different sticking coefficients have been estimated for the film-forming species, as previously mentioned, higher for the O-containing as for the oxygen-free one. Moreover, other important points should be taken into account for plasma polymerization, such as ion bombardment, which transfers kinetic energy to the substrate with consequences for the coating properties [11,12]. Furthermore, in the case of HMDSO plasma polymerization with O_2 in the mixture, the diffusion and reactivity of neutral species at the surface derived from oxygen should also play a role, apart from how they affect the gas chemistry.

A flat substrate located on the electrode is completely exposed to the plasma, directly separated by the plasma sheath. However, complex substrates with an open, porous, or filamentary structure comprise many zones that are not exposed to the plasma. This problem has been studied for decades known as “aperture-well assembly” [13,14] or “cavity technique” [15,16]. The main idea is to use a cavity as an almost closed substrate, only opened to the plasma species by a small opening, usually between 0.1 and 2.5 mm wide. The central objective of these studies was to analyze the surface loss probability, that is, the sum of all the probabilities of effective sticking inside the cavity, including the consequences of surface reactions. Note that, taking into account that the cavity provides a confined space, all entering reactive species will react, either sticking to the surface or forming stable volatile products. This technique has been applied for different PECVD processes such as hydrocarbon plasmas [15] or silane discharges [13]. Taking into account that a significant portion of the substrate is not exposed to the plasma, this area would not see the flux of energetic plasma species (i.e., ions or fast neutrals, among others) [13]. Similarly, metal meshes are used to partially extract charged particles in inductively coupled plasma (ICP) sources: the sheath region ranging over several Debye lengths around the opening attracts charged particles by the electric field force, whereas neutral particles are largely unaffected [17].

Other studies have dealt with the deposition in undercuts [18] or small gaps [19] using fluorocarbon plasmas. In this way, two zones can be differentiated on the substrate, one covered by a (metallic) plate and therefore unexposed to the plasma and the second fully exposed to the plasma. Due to the parallel arrangement forming the undercut, charged particles can be discarded in the unexposed region while diffusion of the residual plasma species (including film-forming species) is the dominant film deposition process [19]. Conversely, for other deposition configurations known as *downstream, remote* or *afterglow* plasmas [14,20,21], also designed to entirely avoid ion-induced effects during film growth, only long-living species from the plasma reach the substrate, thus promoting a kind of radical polymerization.

This article uses cavity and undercut configurations as substrates placed close to the plasma to analyze deposition from HMDSO with and without admixed oxygen. In a simplified way, these substrates mimic complex geometries that could be functionalized with HMDSO-derived plasma polymer films (PPFs). The substrates within the cavity and undercut geometries were located on the bottom electrode of a parallel-plate RF CCP reactor, separated to the active plasma zone only by the plasma sheath and thus directly exposed to all neutral plasma species. The obtained results, focusing on the chemistry of the plasma polymer films, are discussed in terms of the surface reactivity of the film-forming species, considering additional surface reactions when they reach the surface.

2. Materials and methods

The experiments have been carried out in a capacitive coupled radiofrequency (RF) plasma reactor with a parallel-plate configuration (30 cm in diameter, 5 cm distance). The gases enter the chamber through the top electrode and homogeneously diffuse through many holes in the bottom electrode connected to the pumping system. This uniform gas distribution allows a homogeneous deposition rate along the electrodes. The substrates, placed on the bottom electrode, consisted of different materials: p-doped silicon (Si) wafers – to ensure that they are electrically conductive – 60 μm thick polypropylene (PP) foils (Greiner Packaging), and conventional aluminum (Al) foil. While Si wafers were used for profilometry and XPS measurements, PP foil was used for scanning electron microscopy analysis, and Al foil for ATR-FTIR measurements.

Hexamethyldisiloxane (HMDSO, Sigma Aldrich) has been used as monomer. Two kinds of plasma polymerization experiments were performed at 7 Pa: (1) mixtures of HMDSO and argon (Ar) and (2) of HMDSO, Ar, and oxygen (O_2). The flow rate of HMDSO was set as 2 sccm, of Ar as 20 sccm in the former and 10 sccm in the latter case, while the flow rate of O_2 was 20 sccm (1:10 HMDSO to O_2 ratio). Furthermore, etching experiments with 20 sccm Ar (only Ar etching) and 20 sccm Ar + 5 sccm O_2 (Ar/O_2 etching) have been performed at 10 Pa. Note that the operating pressure was managed using valves that regulate the pumping speed. All the experiments – including etching – used continuous applied power of 30 W, yielding representative polydimethylsiloxane (PDMS)-like or SiO_x coatings. For these operating conditions, the deposition rate was 37 $nm{\cdot}min^{-1}$ and 25 $nm{\cdot}min^{-1}$ without and with O_2 added, respectively. The latter is lower since less energy is available per HMDSO molecule due to energy uptake by O_2 activation [4]. Before the plasma polymerization experiments, the substrates were cleaned for 2 min with an Ar/O_2 plasma (20/5 sccm) at 20 W and 7 Pa. A V/I probe (ENI Model 1065) was set close to the bottom electrode to electrically characterize the discharges.

A profilometer (Dektak XT, Bruker) was used to determine the thickness of the coatings. Scanning electron microscopy (SEM, Hitachi S4800) served to analyze the changes in the surface morphology due to etching effects, operating the microscope at 2 kV and detecting secondary electrons. Contact angle was measured in static mode by depositing water drops (2 μl) with a Krüss (DSA25) device.

The chemical composition was analyzed by attenuated total reflection Fourier transform infrared spectroscopy (ATR-FTIR, Varian 640-IR, Agilent Technologies). For comparative purposes, ATR-FTIR absorption spectra are plotted normalized to the Si-O-Si stretching mode (1097 cm^{-1}) for HMDSO polymerization and to the SiO_2 LO mode (1228 cm^{-1}) for O_2/HMDSO polymerization. Furthermore, X-ray photoelectron spectroscopy was also used (XPS). XPS measurements were carried out using a scanning XPS microprobe spectrometer (PHI VersaProbe II, Physical Electronics) with monochromatic Al Kα radiation (1486.6 eV). A photoemission take-off angle of 45° (to the sample surface) was used. The operating pressure of the XPS analysis chamber was below 10^{-6} Pa during the measurements. Survey scan spectra (0 – 1100 eV) were acquired with an energy step size of 0.8 eV, an acquisition time of 200 ms per data point and an analyzer pass energy of 187.85 eV. For the elements, carbon C 1s (276-296 eV), oxygen O 1s (523-543 eV), and silicon Si 2p (92-112 eV), also higher resolution region spectra were acquired with 0.125 eV energy step size, 1.92 s (C, O) and 2.4 s (Si) acquisition time per data point and 29.35 eV analyzer pass energy. The corresponding energy resolution (FWHM) measured on the silver Ag $3d_{5/2}$ photoemission line is 2.2 eV and 0.7 eV for survey and region scans, respectively. Total acquisition times were approximately 5 min for survey scans and 20 min together for the three region scans. XPS analysis was carried out at different surface positions of the samples (attached to

the sample holder via adhesive tape) using a micro-focused X-ray beam with a diameter of 100 μm (25 W at 15 kV). The 180° spherical capacitor energy analyzer was operated in the fixed analyzer transmission (FAT) mode with an analyzer acceptance angle of ± 20°. Possible sample charging was compensated using dual beam charge neutralization with a flux of low energy electrons (1.3 eV) combined with very low energy Ar^+ ions (10 eV).

The obtained XPS spectra were rescaled by shifting them relative to the known binding energy of the C-Si signal (C 1s peak in polydimethylsiloxane) at 284.4 eV [22]. Intensity determination with CasaXPS software version 2.3.16 (Casa Software Ltd) was employed to calculate the atomic concentrations. A mixed Gaussian-Lorentzian product function (constant ratio of 70 % Gaussian and 30 % Lorentzian) was used to curve fitting the XPS spectra for determining the bonding states of C, O, and Si. Thereby, a Shirley type background was subtracted from the XPS peak areas. For quantification, tabulated PHI sensitivity factors [23] corrected for our system's transmission function and analyzer asymmetry parameter (correction due to a different angle between X-ray source and analyzer) have been used. More details about the XPS system have been previously published in [24].

2.1. Description of the substrates: "cavity" and "undercut" configurations

Inspired by the traditional cavity configuration [13,15], we designed two geometries for simplified studies to investigate how plasma polymerization of HMDSO occurs in complex geometries. Fig. 1 shows schemes of these geometries, named "cavity" and "undercut" configurations, as well as the deposition profiles for HMDSO and O_2/HMDSO polymerization. The cavity configuration (Fig. 1**(a)**) consists of two Si wafers (2 cm wide) separated by a slit opening of 2 mm, located 0.6 mm above the bottom material. Additional experiments were performed with smaller openings of 0.5 and 1 mm. Complementarily, the undercut (Fig. 1**(b)**) allows us to distinguish two different regions: one below the undercut, unexposed to the plasma and the ion bombardment, and the other outside the shielding roof made of a 2 cm broad Si wafer, exposed to all plasma species. Another Si wafer was placed at the bottom, covering only the plasma-exposed side, to avoid ions potentially arriving at a small angle to the plasma-shielded zone. It extracted ions by the electric field at its edge directly beneath the upper Si wafer, forming the undercut. Similar configurations have been previously used in the literature, for example by S. Tajima and K. Komvopoulos [18], partially covering the substrate with an aluminum plate placed 2 mm above, defining *shielded* and *unshielded* plasma regions, to prevent ion bombardment and VUV radiation during film growth in the *shielded* part. It is important to note that, different from what has been referred to downstream or remote plasmas [14,20,21], in the undercut configuration, the species from the plasma can effectively enter the unexposed region by diffusion, yet avoiding the contribution of high-energy species.

For both configurations, a Si wafer, a PP, and an Al foil are placed at the bottom of the two configurations for characterization. Note that the plasma ignition in the *cavity* or below the *undercut* is prevented due to their millimeter height above the bottom, smaller than the plasma sheath width at these conditions (around 1 cm) [4]. Fig. 1**(c) and (d)** show the deposition profiles for HMDSO and O_2/HMDSO plasma deposition within the cavity (see also Supplementary Material S1) and the undercut, respectively. The thickness is normalized to the thickness of a coating fully exposed to the plasma (333 nm for 9 min HMDSO plasma and 350 nm for 14 min O_2/HMDSO plasma). It can be observed that, indeed, the film-forming species diffuse through the geometries, detecting coatings of tens of nanometers, millimeters away from the

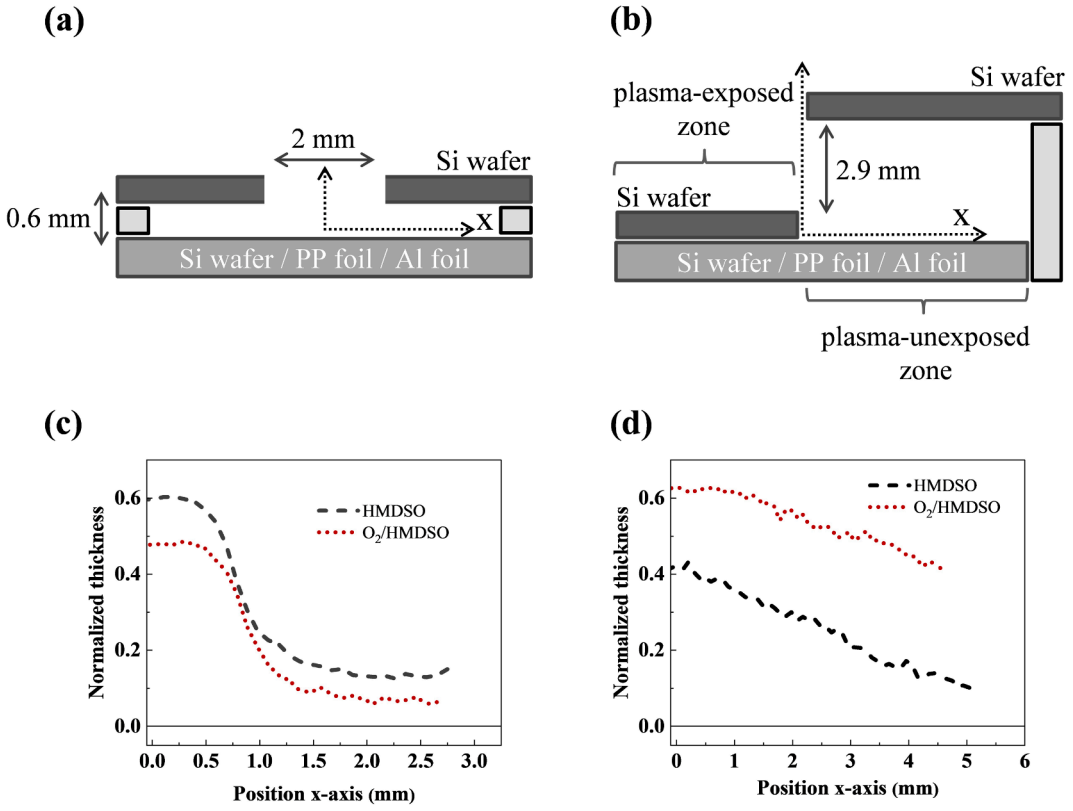

Fig. 1. Scheme of the geometries used as substrates and deposition profiles. (a) Cavity, with an opening of 2 mm on the top part. (b) Undercut, defining plasma unexposed and exposed zones below and outside the undercut, respectively. (c) Deposition profile in the x > 0 zone of the cavity. (d) Deposition profile in the x > 0 zone in the undercut. Note that, for the deposition profiles, the thickness is normalized to the thickness of a coating fully exposed to the plasma (333 nm for the HMDSO case and 350 nm for the O_2/HMDSO case).

opening in both configurations. However, differences can also be noted between the two configurations, showing a more directed deposition for HMDSO and enhanced diffusion for O_2/HMDSO, which will be further discussed below.

3. Results and discussion

3.1. HMDSO plasma polymerization mechanisms

For the examined operating conditions (2 sccm HMDSO, 20 sccm Ar, 7 Pa, 30 W, 10 min), a thickness of 333 nm is measured on a standard Si wafer entirely exposed to the plasma. A lower thickness of around 200 nm is detected in the center of the cavity, decreasing along the x-axis (see Fig. 1**(c)**). In contrast, around 140 nm coating is detected close to the entrance of the undercut (i.e., at the position where the undercut starts; see Fig. 1**(d)**). It is known that, in PECVD processes, not only the diffusion of film-forming species but also the limited mobility of high-energy particles through the geometry is important. Ion bombardment affects plasma polymerization processes, modifying aspects from the deposition rate to the chemistry of the polymer, among others [4,11,12]. The higher deposition rate right underneath the cavity opening with respect to the entrance of the undercut indicates that energetic species might enter the cavity and support the sticking of the molecule fragments by forming nucleation sites [25]. Thus, we wanted to clarify first whether energetic species (ions and fast neutrals by charge exchange) are able to penetrate the cavity while they can be excluded for the undercut configuration. Therefore, additional plasma etching experiments (Ar/O_2 plasma, 30 W, 10 Pa, 30 min) have been carried out with a polypropylene (PP) foil located at the bottom of the cavity. Profilometry measurements of the PP foil centered underneath the middle of the slit have indeed revealed a pronounced etching profile underneath the slit openings (see Supplementary Material S2). The observed trench, imaging the width of the opening, indicates a direct plasma interaction effect; it can thus be inferred that energy is still deposited in the cavity configuration underneath the slit opening. Regarding the evolution of the plasma-etched morphology of PP using SEM analysis [26], the reduction in the etching rate inside the cavity can be investigated compared to a fully plasma-exposed PP surface (see Supplementary Material S3). The as-observed reduction of about 3, 6, and 12 times for the 2, 1, and 0.5 mm slit openings, respectively, demonstrate that a fraction of the high-energy particles can effectively enter into openings equal to or wider than 0.5 mm [27]. This fact might have a consequence on the polymerization mechanisms in the cavity, as will be discussed below.

When igniting an HMDSO/Ar discharge, two main film-forming species are formed: $(CH_3)_x$-Si-O$^{\cdot}$ and $(CH_3)_x$-Si$^{\cdot}$ [4], corresponding to the two fragments of the molecule. Abstracted hydrocarbon radicals tend to recombine with H and form stable volatile products. Therefore, two different film-forming species can be assumed to reach the used geometries and diffuse into them (by gas and surface diffusion). To analyze the chemical composition using ATR-FTIR, an Al foil was used as substrate placed at the bottom part of the two configurations. Fig. 2**(a)** and **(b)** show normalized ATR-FTIR spectra for the cavity and undercut, respectively. In both plots, the spectrum of a plasma polymer film (PPF) deposited in the plasma-exposed zone is included for comparison. On the one hand, vibration modes associated with PDMS are observed in the spectra, from lower to higher wavelengths, with bands assigned to Si-O-R and Si-O-Si stretching vibrations at 1016 and 1097 cm^{-1}, respectively, and the δ (Si-CH_3) vibration mode at 1259 cm^{-1}. Related to the δ (Si-CH_3) vibration, the CH_3 asymmetric stretch is also detected at 2960 cm^{-1} [28]. On the other hand, contributions of the SiO_2 (TO and LO) asymmetric modes at 1074 and 1228 cm^{-1}, respectively, cannot be discarded [29]. For both configurations, the same tendency is found: with increasing distance from the center of the cavity (Fig. 2**(a)**, x = 4 mm) or from the entrance of the undercut (Fig. 2**(b)**, x ≥ 0), the intensity of the δ (Si-CH_3) band (as well as that of the CH_3 stretch) increases with

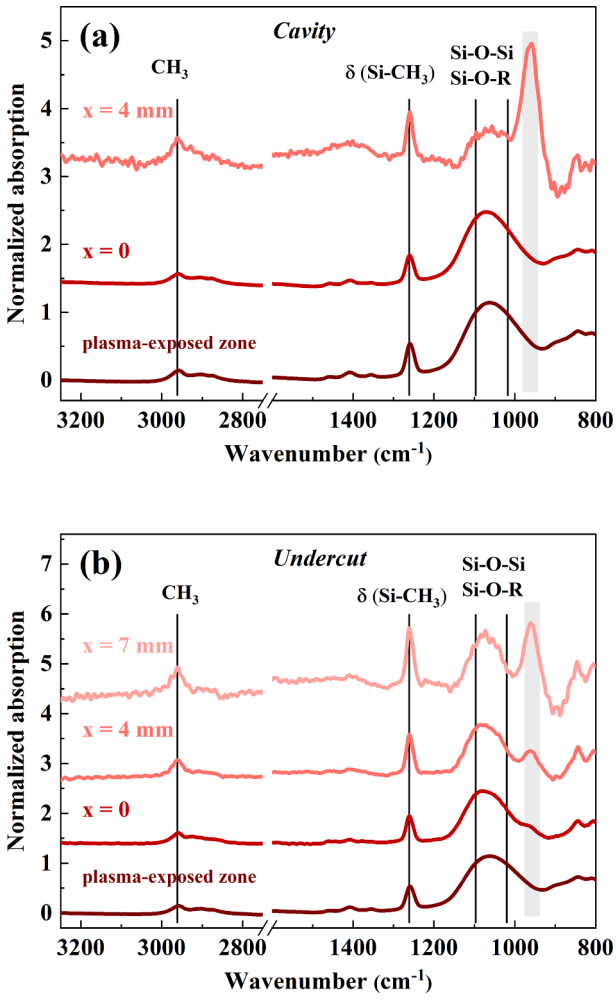

Fig. 2. ATR-FTIR analysis of PPFs obtained from HMDSO plasma polymerization using the (a) cavity and the (b) undercut configuration with an Al foil on the bottom. Vibration bands associated with the PPF are indicated with black solid lines. The intensity has been normalized to that of the 1097 cm^{-1} band (Si-O-Si stretching vibration). A band appearing at 980 cm^{-1}, attributed to the oxidation of the aluminum substrate, is indicated with a gray stripe. The region between 2800 and 1800 cm^{-1} is hidden due to the absence of any signal to better observe the other regions (see Supplementary Material S4 for the entire spectra).

respect to that of the Si-O-R/Si-O-Si/SiO_2 bands. An additional signal appears at 980 cm^{-1}, marked with a gray stripe in the plot, which does not correspond to the PPF but to the oxidation of the Al substrate. Note that this band is observed when the thickness of the coating is decreasing and becomes dominant for a thickness below 10 nm, as at position x = 4 mm in the cavity and x ≥ 4 mm in the undercut (see Fig. 1). Additionally, small differences can be inferred by comparing the spectrum of the plasma-exposed zone to those for the undercut for x ≥ 0, with a narrowing of the 1150–1000 cm^{-1} region related to the absence of ion bombardment below the undercut. See Supplementary Material S4 for the entire spectra, where the Si-OH and OH bands can also be observed. Note that, in these spectra, the intensity has been normalized to the Si-O-Si signal at 1097 cm^{-1}. This band is generally close to having the highest intensity, except for very thin coatings far away from the opening where the contribution of the oxidized substrate arises.

The relatively increasing intensity of the δ (Si-CH_3) band with respect to the Si-O bonds in the plasma-shielded regions indicates different sticking probabilities of the two film-forming species, $(CH_3)_x$-Si-O$^{\cdot}$ and $(CH_3)_x$-Si$^{\cdot}$, with a higher sticking coefficient for the former. Hence, the $(CH_3)_x$-Si-O$^{\cdot}$ fragments rapidly stick and get deposited close to the

entrance of the geometries dominating film growth. Comparing plasma-exposed spectra to spectra at x = 0 for cavity and undercut show that the deposited energy has a minor effect on chemistry. $(CH_3)_x$-Si· fragments with lower reactivities diffuse through the geometry and contribute to the film composition when the former species become depleted, yielding an almost linear reduction in deposition rate within the undercut. Accordingly, a correlation with the evolution of the chemical composition along the x-axis is found for the PPFs analyzed by XPS, further discussed below. Taking into account that O_2 has not been added to the plasma, additional surface oxidation reactions have not been considered to take place.

3.2. HMDSO & O_2 plasma polymerization mechanisms

When O_2 is added to the plasma, the oxygen-free fragment arising from HMDSO activation, $(CH_3)_x$-Si·, might react with atomic oxygen yielding essentially $(CH_3)_x$-Si-O· as the only species contributing to the growth of the film. Fig. 3 shows normalized ATR-FTIR spectra for the **(a)** cavity and **(b)** undercut configurations for plasma polymerization with an O_2/HMDSO ratio of 10:1 (experimental conditions: 10 sccm Ar, 20 sccm O_2, 2 sccm HMDSO, 7 Pa, 30 W, 14 min). In this case, the thickness of the PPF in the exposed plasma zone was 350 nm. Enhanced penetration of the film-forming species can be inferred, since, for the cavity and the undercut, distinct film formation has been detected by ATR-FTIR at positions 7 and 11 mm to the center, respectively, higher than at 4 and 7 mm for the HMDSO plasma without O_2 addition.

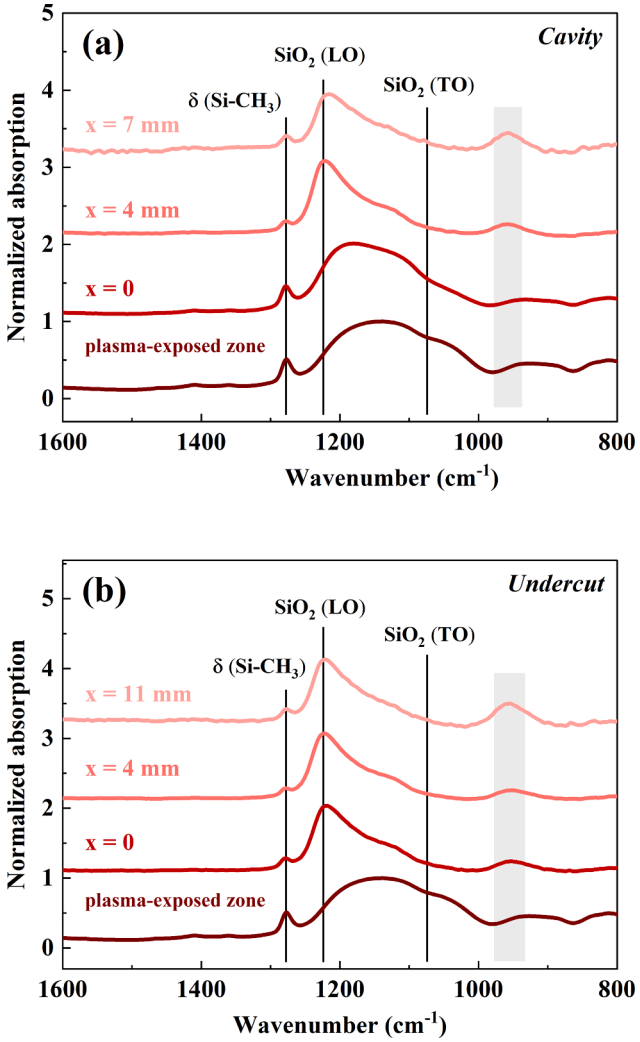

Fig. 3. ATR-FTIR analysis of PPFs obtained from O_2/HMDSO plasma polymerization using the (a) cavity and the (b) undercut as substrates with an Al foil on the bottom. Vibration bands associated to the PPF are indicated with black solid lines. The intensity has been normalized to the highest recorded peak in each case, close to the signal of the SiO_2 LO mode (1228 cm^{-1}). A band appearing at 980 cm^{-1}, attributed to the oxidation of the aluminum substrate, is indicated with a gray stripe. The region between 3200 and 1600 cm^{-1} is hidden to better observe the other regions (see Supplementary Material S5 for the entire spectra).

In Fig. 3, the δ (Si-CH_3) band is detected at 1259 cm^{-1}, while the aforementioned asymmetric stretching vibrations of SiO_2 are detected by their LO (1228 cm^{-1}) and TO (1074 cm^{-1}) modes [29]. Note that all spectra shown in the figure are normalized to the highest intensity recorded in each case, which corresponds to a position close to the LO mode (1228 cm^{-1}). Entering the plasma-shielded zone, all spectra show a similar tendency: the intensity of the δ (Si-CH_3) band slightly decreases (contrary to for HMDSO plasmas) and the LO mode of SiO_2 becomes dominant while the TO mode tends to disappear. Recall that $(CH_3)_x$-Si-O· is the dominant film-forming radical with high sticking probability, likely to be deposited close to the entrance of the exposed-plasma zones as observed for the case without O_2 addition. Due to the enhanced penetration, it is thus reasonable to assume that $(CH_3)_x$-Si· radicals are not oxidized in the gas phase but rather at the surface by reacting with diffusing reactive oxygen species. Small but clear differences can be observed between the plasma exposed PPF and the x = 0 positions in both configurations, again depending on the reduced energetic bombardment: the SiO_2 bands shift to higher wavenumbers, associated with the LO mode. This behavior is pronounced when the PPF is located in the unexposed zones where no ion bombardment occurs. This narrowing of the SiO_2 band can be related to chemical etching (removal of hydrocarbons) and oxidation occurring at the surface, due to atomic oxygen (and probably further reactive oxygen species) diffusing and reacting with the film-forming species at the surface. It should be considered that the thinner the coating is, the longer the interaction time with the oxygen species. This might well explain why the narrowing effect is more pronounced farther away from the opening. Similarly to HMDSO plasma polymerization, the aluminum oxide band appears at 980 cm^{-1} when the coating becomes very thin, that is, for $x \geq 4$ mm for the cavity and $x \geq 7$ mm for the undercut. Note, however, that in this experiment, the oxidation of the substrate might be enhanced due to the presence of O_2 in the admixture and the corresponding chemical etching effects.

A similar narrowing of the Si-O-Si bands has been reported by different authors: for example, in the context of low-k SiCOH materials [5,30] or porous SiO_2 films [31]. Moreover, in a previous study of our research group, a less pronounced but similar tendency for nanoporous SiO_x coatings has been observed deposited by alternating deposition/etching experiments with HMDSO and O_2 [32]. The results shown in Fig. 3 clearly reveal the importance of chemical etching (i.e., surface reactions) in plasma polymerization when complex geometries are used as substrates, an effect that, in this case, appears to be even more pronounced than that of the ion bombardment. The film-forming species produced in the gas phase, $(CH_3)_x$-Si-O· and $(CH_3)_x$-Si· reach the surface and then get oxidized. According to these results and others reported in the literature [33–37], O_2/HMDSO plasma polymerization seems to be a clear combination of gas phase processes and surface reactions, and neither the former nor the latter should be disregarded.

Along these lines, the different tendencies in deposition rates inside the two geometries for O_2/HMDSO plasmas compared to HMDSO as shown in Fig. 1**(c,d)** might be understood. The interaction with active oxygen species at the surface and chemical etching result in a more diffusive, less directed deposition allowing enhanced penetration.

To further probe the role of chemical etching due to diffusion of oxygen species through the geometries, additional plasma etching experiments were carried out in the undercut (Ar/O_2 plasma, 30 W, 10 Pa, 30 min), similarly to what has been discussed in **section 3.1** for the cavity. As previously described, the undercut configuration is well suited

to avoid ion bombardment. For a similar configuration using a C_4F_8 plasma, Tajima and Komvopoulos affirmed that more than 90 % of the ions are adsorbed or scattered, leaving merely uncharged particles to contribute to the polymerization along the undercut [18]. Fig. 4 shows SEM pictures of PP foils located at different positions in the undercut after plasma exposure. The morphology of an etched PP can be observed for the foil located in the plasma-exposed zone (Fig. 4(a), $x < 0$), related to the removal of the amorphous phase of the polymer [38]. However, a transition pattern can be observed when entering the undercut ($x \geq 0$, Fig. 4**(b)**), where ion effects are strongly reduced, and observing a clear different pattern as a consequence of chemical etching due to surface reactions with diffused oxygen species far from the opening ($x \gg 0$, c.f. Fig. 4**(c)**).

To affirm that this chemical etching is independent of physical effects such as energy deposited by Ar^+ ions or fast Ar neutrals, a parallel experiment was carried out for the undercut configuration exposed to a pure Ar plasma. The corresponding SEM micrographs, shown in Supplementary Material S6 compared to those of the Ar/O_2 plasma, reveal the absence of characteristic etching patterns for the foil below the undercut ($x \geq 0$), showing a similar topography to that of an untreated PP foil [38].

3.3. XPS analysis of the cavity for HMDSO and O_2/HMDSO plasma polymerization

To support the ideas discussed above, XPS analysis for the cavity configuration for HMDSO and O_2/HMDSO plasma polymerization are presented using Si wafers as substrates at the bottom of the cavity. Survey scans (see Supplementary Material S7) depict, as expected, the elements carbon (C), oxygen (O), and silicon (Si). Films located in the plasma-exposed zone were analyzed as references. For the HMDSO deposition, carbon is mostly present in the form of C-Si bonds (binding energy position set to the reference value of 284.4 eV [22]), considering the relative contribution of adventitious C–C (and C–H) to be less than 10 % in the PDMS-like environment. Oxygen is mostly present in the form of $Si(-O)_1$ and $Si(-O)_2$, taken together as one band, 532.2-532.5 eV. With the addition of oxygen in the O_2/HMDSO process (ratio of 10:1), the higher-lying components become dominant, i.e. $Si(-O)_3$ and $Si(-O)_4$ (532.8-533.8 eV). Evidently, the presence of oxygen led to a significantly increased incorporation of oxygen at the expense of (hydro)carbon. In order to derive the chemical composition from the silicon signal, the Si 2p spectral envelope was fitted with the four $Si(-O)_x$ components: $Si(-O)_1$ (101.5 eV), $Si(-O)_2$ (102.1 eV), $Si(-O)_3$ (102.8 eV), $Si(-O)_4$ (103.4 eV) [39]. Mostly, the number of oxygen atoms bonded to silicon will determine the binding energy of the Si 2p peak, with minor binding energy shifts resulting from the carbon and hydrogen bonded atoms to fulfill the bonding requirements of silicon [40]. While for the HMDSO plasma polymer film, the lower oxidized silicon atoms form the major part of the signal envelope, the coating derived from the O_2/HMDSO discharge only contains silicon in the two highest oxidation states.

Fig. 5 shows high-resolution spectra of C 1s, O 1s, and Si 2p for **(a-c)** HMDSO and **(d-f)** O_2/HMDSO plasma polymerization. The spectra corresponding to the center of the cavity (curves $x = 0$) are similar to those of the two reference samples, in agreement with results from ATR-FTIR spectra in Fig. 3**(a)** and **4(a)**: the presence of high-energy particle flux in the region below the opening of 2 mm, although reduced, results in a similar polymerization mechanism in the center of the cavity. It can be easily observed from Fig. 5**(a)** and **(d)** that the amount of carbon is higher in the former case (HMDSO plasma) than in the latter one (O_2/HMDSO plasma). For a deeper investigation of the chemistry along this lateral gradient (*x*-axis dependent), the O 1s (see Fig. 5**(b)** and **(e)**) and Si 2p (see Fig. 5**(c)** and **(f)**) high-resolution scans were analyzed. For the PPF derived from HMDSO, a shift towards lower binding energies for O 1s (Fig. 5**(b)**) as well as Si 2p (Fig. 5**(c)**) occurs, representing an increased amount of the lower oxidized silicon atoms $Si(-O)_1$ and $Si(-O)_2$. The amount of these two components compared to the total oxidized silicon (i.e., $[Si(-O)_1 + Si(-O)_2]/[Si(-O)_1 + Si(-O)_2 + Si(-O)_3 + Si(-O)_4]$) is given in Table 1. For the PPF derived from HMDSO and O_2, only minor binding energy shifts were observed. The chemistry along the *x*-axis indicates a film composed of nearly only the two highest oxidized silicon atom states, i.e. $Si(-O)_3$ and $Si(-O)_4$ (see Table 1**)**. Slightly from 3 mm away from the center of the opening, and clearly from 4 mm ($x = 4$ mm), the background shape was changing (see Supplementary Material S7) pointing towards a layered structure, and a splitting of the silicon peak was observed due to a signal from elemental silicon Si(0) (see Fig. 5**(c)** and **(f)**), indicating that the Si wafer substrate was also detected. This effect is less pronounced for the O_2/HMDSO plasma polymerization (Fig. 5**(f)**), in agreement with the higher penetration of the coating that has been discussed for this case.

Table 1 lists the oxygen-to-carbon ratio (O/C) as well as the ratio of the $Si(-O)_{1,2}$ oxidation states to all oxidized silicon ($Si(-O)_{1,2,3,4}$). Data are provided for the reference sample (plasma-exposed zone) and the different positions measured inside the cavity. For the HMDSO-derived PPF, the O/C ratio decreases along the *x*-axis due to an increasing amount of carbon at the expense of oxygen, in agreement with Fig. 3**(a)** indicating a higher mobility for the $(CH_3)_x$-$Si^{\cdot}$ film-forming species compared to those containing oxygen. Furthermore, a slight increase in the $Si(-O)_{1,2}$ with respect to $Si(-O))_{1,2,3,4}$ is noted. Contrary to the HMDSO plasma, oxygen addition results in an increase of the O/C ratio along the *x*-axis, in agreement with Fig. 4**(a)**. As discussed, the chemical etching taking place inside the cavity causes a more inorganic SiO_2-type coating in the plasma-shielded region. Accordingly, the $Si(-O)_{1,2}$ to $Si(-O)_{1,2,3,4}$ ratio is almost zero for the reference sample and the different *x*-positions. As previously mentioned, for both plasma polymerization cases at $x = 4$ mm (and slightly for $x = 3$ mm) signals from the substrate are detected, affecting the ratios as summarized in Table 1.

3.4. Summarizing discussion

The differences in the chemical composition (XPS and ATR-FTIR analysis) reveal that the PPFs deposited inside the cavity or below the undercut can be distinguished by different local properties. This is an important aspect taking into account that PPFs obtained from HMDSO can be proposed for cutting-edge applications such as functional layers in biomaterials, a field usually characterized by 3D geometries. Their diverse properties obtained depending on the operating conditions, the fact that they are deposited at room temperature, or their resistance to oxidizing conditions make them interesting for bioapplications such as, for example, functionalization of catalytic metal oxides, as recently reported by our research group [41]. Surface wettability, a synergistic consequence of the morphology at the nanoscale and the chemical composition, is one important property of advanced functional materials [42]. The water contact angle obtained for a film completely exposed to the plasma was 95° and 81° for HMDSO and O_2/HMDSO (10:1) plasmas, respectively. In the former case, the value increased up to 102° inside the cavity and below the undercut, due to the higher presence of CH_3 groups, which are related to a more hydrophobic behavior [42]. On the

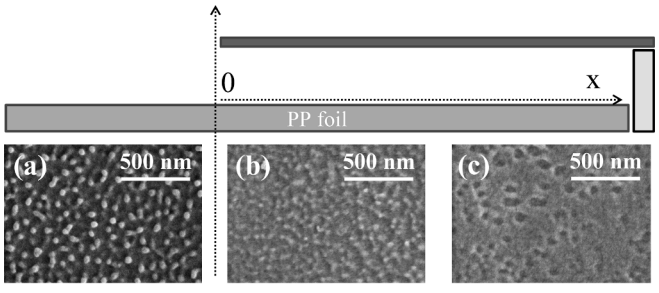

Fig. 4. SEM images of etched PP foils after an Ar/O_2 plasma (30 W, 10 Pa, 30 min) for different positions in the undercut: (a) plasma-exposed zone, (b) $x \geq 0$, and (c) $x \gg 0$.

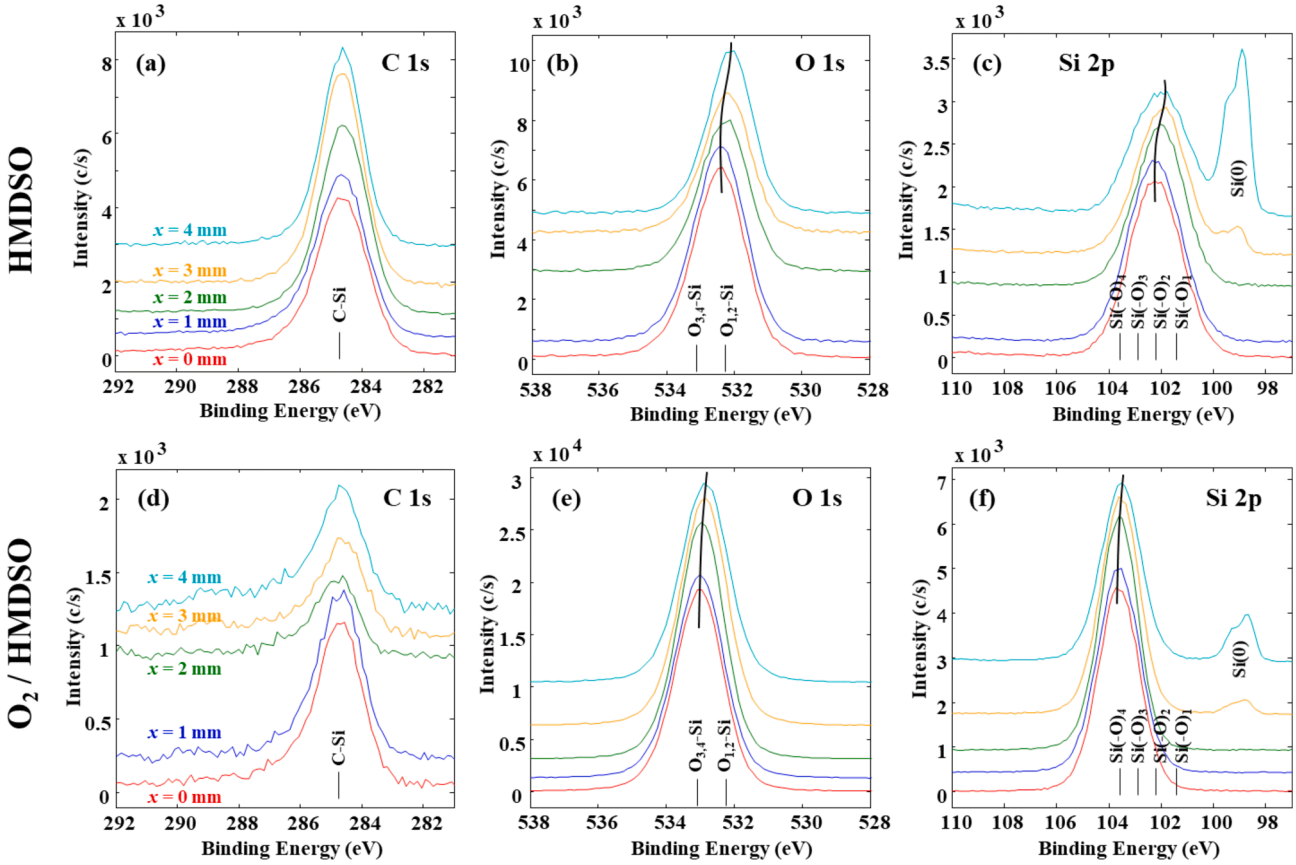

Fig. 5. XPS high-resolution spectra for the coatings derived from (a-c) HMDSO and (d-f) HMDSO and O_2. (a, d) C 1s; (b, e) O 1s, and (c, f) Si 2p. The individual spectra (offset in the y-direction) are taken along the *x*-axis positions of $x = 0$, 1, 2, 3, and 4 mm to the center of the cavity. The components are given above the binding energy scale, which was calibrated by setting the C-Si component to the known binding energy of 284.4 eV. The thicker lines show the trend in binding energy shift for the oxygen and silicon peaks along the gradient in the *x*-axis.

Table 1
Determination of the O/C ratio and the portion of the two lower-lying oxidized silicon peaks ($Si(-O)_{1,2}$) compared to all oxidized silicon ($Si(-O)_{1,2,3,4}$) for the reference sample and for different positions in the cavity along the *x*-axis. Note that, at $x = 4$ mm, contributions from the silicon substrate are detected.

Sample/position	HMDSO plasma		O_2/HMDSO plasma	
	O/C *	$Si(-O)_{1,2}/Si(-O)_{1,2,3,4}$ **	O/C*	$Si(-O)_{1,2}/Si(-O)_{1,2,3,4}$ **
Reference (plasma-exposed)	0.55	0.75	6.4	0.00
$x = 0$ mm	0.58	0.70	5.5	0.00
$x = 1$ mm	0.61	0.72	6.1	0.00
$x = 2$ mm	0.37	0.80	9.3	0.00
$x = 3$ mm	0.31	0.85	10.9	0.00
$x = 4$ mm	0.39	0.68	8.8	0.03

* The error in the O/C ratio is ± 0.02 and ± 1.0 for HMDSO and O_2/HMDSO, respectively.
** The error in the $Si(-O)_{1,2}/Si(-O)_{1,2,3,4}$ ratio is ± 0.03 for both cases.

other hand, for the O_2/HMDSO plasma polymerization, the contact angle decreases to 65° for the zones away from the plasma-exposed zone. This absence of homogeneity might be regarded as a disadvantage if the interest is obtaining a homogeneous material, but also as an advantage if the purpose lies in gradient coatings with controlled properties in certain directions [43,44]. Moreover, the plasma conditions might be adjusted, e.g., by reducing ion bombardment or enhancing O_2 admixture to balance the observed differences between plasma exposure and shielded areas. As an important difference between HMDSO plasma polymerization with and without oxygen admixture, the enhanced diffusion and penetration into plasma-shielded regions is demonstrated. Film-forming species generated in the HMDSO plasma need to be sufficiently active, i.e. forming O-Si-CH and Si-CH bi-radicals, to deposit when energetic plasma interaction is absent yielding a more directed deposition. Generation of reactive oxygen species, on the contrary, yield oxidation effects in shielded regions affecting plasma polymerization at the surface. The results reported in this study disclose the importance to analyze plasma polymerization in the cavity or undercut geometries if one moves from flat substrates to complex 3D geometries, an aspect that already is and surely will have a crucial role in the near future.

4. Conclusions

Two configurations have been designed to analyze PECVD processes in complex geometries, named as cavity and undercut. They consist of (1) a cavity with a 2 mm slit opening on the top and (2) an undercut made by a 3 mm height roof, several mm long. Ar/O_2 plasma etching experiments were carried out to simulate the bombardment of high-energy particles and chemical etching conditions in both configurations using polypropylene foils as substrates. The obtained data reveal that energetic particles can effectively enter small openings exposed to the plasma, albeit with a reduction in their energy-delivering effect. In the regions that are not exposed to the plasma, a chemical etching caused by oxygen species diffusing into the geometries has been detected and distinguished from plasma-assisted effects through high-energy particles.

The plasma polymerization mechanisms in HMDSO/Ar and HMDSO/Ar/O_2 plasmas have been analyzed within the cavity and the undercut.

The analysis of the chemical composition of the plasma polymer films (PPFs) by ATR-FTIR and XPS indicate that, for the PPFs derived from HMDSO plasma polymerization, film-forming species free of oxygen are characterized by a lower sticking coefficient able to diffuse and be deposited farther in the plasma-shielded region, while those containing oxygen are more reactive and mainly deposit close to the plasma-exposed zone. For the O_2/HMDSO plasma polymerization, an important role of reactive oxygen species has been revealed: the less reactive initially oxygen-free film-forming species that are diffusing into the geometries get oxidized and activated at the surface, thus enhancing penetration into complex geometries. Furthermore, the surface reactivity of oxygen species (i.e., chemical etching) allows the deposition of more inorganic coatings in the unexposed-plasma region, close to SiO_2-type PPFs despite of the moderate O_2/HMDSO ratio of 10:1 in the plasma.

The results obtained in this study directs attention to changing conventional 2D perspectives to 3D in order to effectively apply PECVD processes for advanced applications where complex 3D materials are used as substrates.

CRediT authorship contribution statement

Paula Navascués: Conceptualization, Investigation, Data curation, Formal analysis, Writing - original draft, Writing - review & editing. **Martina Buchtelová:** Investigation, Data curation, Formal analysis, Writing - review & editing. **Lenka Zajícková:** Supervision, Funding acquisition, Writing - review & editing. **Patrick Rupper:** Investigation, Data curation, Formal analysis, Writing - review & editing. **Dirk Hegemann:** Supervision, Conceptualization, Funding acquisition, Writing - review & editing.

Declaration of Competing Interest

The authors declare that they have no known competing financial interests or personal relationships that could have appeared to influence the work reported in this paper.

Data availability

Data will be made available on request.

Acknowledgements

P. Navascués and D. Hegemann acknowledge funding by SNSF (Switzerland, COST 2022, project 213368). M. Buchtelová and L. Zajícková acknowledge funding by the Czech Science Foundation (project 21-12132J) and the Specific Research Projects (project CEITEC VUT-J-23-8335).

Appendix A. Supplementary data

Supplementary data to this article can be found online at https://doi.org/10.1016/j.apsusc.2023.158824.

References

[1] H.K. Yasuda, Plasma Polymerization, Academic Press, 2012.
[2] R. d'Agostino, Plasma Deposition, Treatment, and Etching of Polymers: The Treatment and Etching of Polymers, Elsevier Science, 1990.
[3] N. Inagaki, Plasma surface modification and plasma polymerization, CRC press, Boca Raton (2014), https://doi.org/10.1201/9781498710831.
[4] D. Hegemann, E. Bülbül, B. Hanselmann, U. Schütz, M. Amberg, S. Gaiser, Plasma polymerization of hexamethyldisiloxane: Revisited, Plasma Process Polym. 18 (2021) 2000176, https://doi.org/10.1002/ppap.202000176.
[5] A. Grill, Porous pSiCOH ultralow-*k* dielectrics for chip interconnects prepared by PECVD, Annu. Rev. Mater. Res. 39 (2009) 49–69, https://doi.org/10.1146/annurev-matsci-082908-145305.
[6] K. Arts, S. Hamaguchi, T. Ito, K. Karahashi, H.C.M. Knoops, A.J.M. Mackus, W.M. M. (Erwin) Kessels, Foundations of atomic-level plasma processing in nanoelectronics, Plasma Sources Sci. Technol. 31 (2022) 103002, https://doi.org/10.1088/1361-6595/ac95bc.
[7] M. Michlíček, L. Blahová, E. Dvořáková, D. Nečas, L. Zajíčková, Deposition penetration depth and sticking probability in plasma polymerization of cyclopropylamine, Appl. Surf. Sci. 540 (2021) 147979, https://doi.org/10.1016/j.apsusc.2020.147979.
[8] A.G. Guex, D. Hegemann, M.N. Giraud, H.T. Tevaearai, A.M. Popa, R.M. Rossi, G. Fortunato, Covalent immobilisation of VEGF on plasma-coated electrospun scaffolds for tissue engineering applications, Colloids Surf. B Biointerfaces 123 (2014) 724–733, https://doi.org/10.1016/j.colsurfb.2014.10.016.
[9] T.I.U. of P. and A. Chemistry (IUPAC), IUPAC - sticking coefficient (S06012), (n.d.). https://doi.org/10.1351/goldbook.S06012.
[10] M. Bauer, T. Schwarz-Selinger, W. Jacob, A. von Keudell, Growth precursors for a-C: H film deposition in pulsed inductively coupled methane plasmas, J. Appl. Phys. 98 (2005) 073302, https://doi.org/10.1063/1.2061890.
[11] D. Hegemann, Plasma Polymer Deposition and Coatings on Polymers, Comprehensive Materials Processing 4 (2014) 201–228. doi:10.1016/B978-0-08-096532-1.00426-X.
[12] R. Snyders, D. Hegemann, D. Thiry, O. Zabeida, J. Klemberg-Sapieha, L. Martinu, Foundations of plasma enhanced chemical vapor deposition of functional coatings, Plasma Sources Sci. Technol. 32 (2023) 074001, https://doi.org/10.1088/1361-6595/acdabc.
[13] D.A. Doughty, J.R. Doyle, G.H. Lin, A. Gallagher, Surface reaction probability of film-producing radicals in silane glow discharges, J. Appl. Phys. 67 (1990) 6220–6228, https://doi.org/10.1063/1.345188.
[14] W.M.M. Kessels, M.C.M. Van De Sanden, R.J. Severens, D.C. Schram, Surface reaction probability during fast deposition of hydrogenated amorphous silicon with a remote silane plasma, J. Appl. Phys. 87 (2000) 3313–3320, https://doi.org/10.1063/1.372342.
[15] C. Hopf, T. Schwarz-Selinger, W. Jacob, A. Von Keudell, Surface loss probabilities of hydrocarbon radicals on amorphous hydrogenated carbon film surfaces, J. Appl. Phys. 87 (2000) 2719–2725, https://doi.org/10.1063/1.372246.
[16] C. Hopf, K. Letourneur, W. Jacob, T. Schwarz-Selinger, A. Von Keudell, Surface loss probabilities of the dominant neutral precursors for film growth in methane and acetylene discharges, Appl. Phys. Lett. 74 (1999) 3800–3802, https://doi.org/10.1063/1.124184.
[17] Y. He, W. Jin, Y. Wang, S. Lv, R. Wang, J. Liu, H. Liu, Electron density and electron temperature control with a magnetic field and a grid in inductively coupled argon plasma, Plasma Chem Plasma Process. 43 (2023) 381–400, https://doi.org/10.1007/s11090-022-10295-7.
[18] S. Tajima, K. Komvopoulos, Physicochemical properties and morphology of fluorocarbon films synthesized on crosslinked polyethylene by capacitively coupled octafluorocyclobutane plasma, J. Phys. Chem. C. 111 (2007) 4358–4367, https://doi.org/10.1021/jp067521e.
[19] L. Zheng, L. Ling, X. Hua, G.S. Oehrlein, E.A. Hudson, Studies of film deposition in fluorocarbon plasmas employing a small gap structure, J. Vac. Sci. Technol. A 23 (2005) 634–642, https://doi.org/10.1116/1.1931680.
[20] J.M. Obrero-Perez, L. Contreras-Bernal, F. Nuñez-Galvez, J. Castillo-Seoane, K. Valadez-Villalobos, F.J. Aparicio, J.A. Anta, A. Borras, J.R. Sanchez-Valencia, A. Barranco, Ultrathin plasma polymer passivation of perovskite solar cells for improved stability and reproducibility, Adv. Energy Mater. 12 (2022) 2200812, https://doi.org/10.1002/aenm.202200812.
[21] D. Theirich, C.h. Soll, F. Leu, J. Engemann, Intermediate gas phase precursors during plasma CVD of HMDSO, Vacuum 71 (2003) 349–359, https://doi.org/10.1016/S0042-207X(02)00763-7.
[22] High Resolution XPS of Organic Polymers: The Scienta ESCA300 Database (Beamson, G.; Briggs, D.), J. Chem. Educ. 70 1993 A25 10.1021/ed070pA25.5.
[23] J.F. Moulder, W.F. Stickle, P.E. Sobol, K.D. Bomben, Handbook of X-ray Photoelectron Spectroscopy, Perkin-Elmer Corporation, Physical Electronics Division, Eden Prairie, MN, USA, 1995.
[24] P. Rupper, M. Amberg, D. Hegemann, M. Heuberger, Optimization of mica surface hydroxylation in water vapor plasma monitored by optical emission spectroscopy, Appl. Surf. Sci. 509 (2020) 145362, https://doi.org/10.1016/j.apsusc.2020.145362.
[25] D. Hegemann, Macroscopic investigation of reaction rates yielding plasma polymer deposition, J. Phys. D: Appl. Phys. 46 (2013) 205204, https://doi.org/10.1088/0022-3727/46/20/205204.
[26] S. Kim, J.-H. Oh, C.H. Park, Development of energy-efficient superhydrophobic polypropylene fabric by oxygen plasma etching and thermal aging, Polymers 12 (2020) 2756, https://doi.org/10.3390/polym12112756.
[27] M. Zelzer, D. Scurr, B. Abdullah, A.J. Urquhart, N. Gadegaard, J.W. Bradley, M. R. Alexander, Influence of the plasma sheath on plasma polymer deposition in advance of a mask and down pores, J. Phys. Chem. B. 113 (2009) 8487–8494, https://doi.org/10.1021/jp902137y.
[28] I.F. Husein, C. Chan, S. Qin, P.K. Chu, The effect of high-dose nitrogen plasma immersion ion implantation on silicone surfaces, J. Phys. D: Appl. Phys. 33 (2000) 2869, https://doi.org/10.1088/0022-3727/33/22/301.
[29] C. Hoppe, F. Mitschker, P. Awakowicz, D. Kirchheim, R. Dahlmann, T. De Los Arcos, G. Grundmeier, Adhesion of plasma-deposited silicon oxide barrier layers on PDMS containing polypropylene, Surf. Coat. Technol. 335 (2018) 25–31, https://doi.org/10.1016/j.surfcoat.2017.12.015.
[30] A. Grill, D.A. Neumayer, Structure of low dielectric constant to extreme low dielectric constant SiCOH films: Fourier transform infrared spectroscopy characterization, J. Appl. Phys. 94 (2003) 6697–6707, https://doi.org/10.1063/1.1618358.

[31] T. De Los Arcos, H. Müller, F. Wang, V.R. Damerla, C. Hoppe, C. Weinberger, M. Tiemann, G. Grundmeier, Review of infrared spectroscopy techniques for the determination of internal structure in thin SiO_2 films, Vib. Spectrosc 114 (2021), 103256, https://doi.org/10.1016/j.vibspec.2021.103256.
[32] T. Gergs, C. Monti, S. Gaiser, M. Amberg, U. Schütz, T. Mussenbrock, J. Trieschmann, M. Heuberger, D. Hegemann, Nanoporous SiOx plasma polymer films as carrier for liquid-infused surfaces, Plasma Processes Polym. 19 (2022) 2200049, https://doi.org/10.1002/ppap.202200049.
[33] D. Hegemann, U. Vohrer, C. Oehr, R. Riedel, Deposition of SiOx films from O_2/HMDSO plasmas, Surf. Coat. Technol. 116–119 (1999) 1033–1036, https://doi.org/10.1016/S0257-8972(99)00092-4.
[34] C. Hoppe, F. Mitschker, I. Giner, T. De Los Arcos, P. Awakowicz, G. Grundmeier, Influence of organic surface chemistry on the nucleation of plasma deposited SiO_x films, J. Phys. D: Appl. Phys. 50 (2017) 204002, https://doi.org/10.1088/1361-6463/aa69e5.
[35] D. Loffhagen, M.M. Becker, A.K. Czerny, J. Philipp, C.-P. Klages, Impact of hexamethyldisiloxane admixtures on the discharge characteristics of a dielectric barrier discharge in argon for thin film deposition, Contributions to Plasma Physics. 58 (2018) 337–352, https://doi.org/10.1002/ctpp.201700060.
[36] K. Rügner, R. Reuter, D. Ellerweg, T. De Los Arcos, A. Von Keudell, J. Benedikt, Insight into the reaction scheme of SiO_2 film deposition at atmospheric pressure: Insight into the reaction scheme of SiO_2 film deposition, Plasma Process Polym. 10 (2013) 1061–1073, https://doi.org/10.1002/ppap.201300059.
[37] S. Guo, W.J. van Ooij, Kinetics of DC discharge plasma polymerization of hexamethyldisiloxane and pyrrole, Plasma Polym. 3 (1998) 1–21, https://doi.org/10.1023/A:1022544132520.
[38] M. Amberg, M. Höhener, P. Rupper, B. Hanselmann, R. Hufenus, S. Lehner, E. Perret, D. Hegemann, Surface modification of recycled polymers in comparison to virgin polymers using Ar/O_2 plasma etching, Plasma Processes Polym. 19 (2022) 2200068, https://doi.org/10.1002/ppap.202200068.
[39] M.R. Alexander, R.D. Short, F.R. Jones, W. Michaeli, C.J. Blomfield, A study of HMDSO/O2 plasma deposits using a high-sensitivity and -energy resolution XPS instrument: curve fitting of the Si 2p core level, Appl. Surf. Sci. 137 (1999) 179–183, https://doi.org/10.1016/S0169-4332(98)00479-6.
[40] E. Vassallo, A. Cremona, L. Laguardia, E. Mesto, Preparation of plasma-polymerized SiOx-like thin films from a mixture of hexamethyldisiloxane and oxygen to improve the corrosion behaviour, Surf. Coat. Technol. 200 (2006) 3035–3040, https://doi.org/10.1016/j.surfcoat.2004.11.001.
[41] D. Hegemann, B. Hanselmann, F. Zuber, F. Pan, S. Gaiser, P. Rupper, K. Maniura-Weber, K. Ruffieux, Q. Ren, Plasma-deposited AgOx -doped TiOx coatings enable rapid antibacterial activity based on ROS generation, Plasma Processes Polym. 19 (2022) 2100246, https://doi.org/10.1002/ppap.202100246.
[42] C. Ma, A. Nikiforov, D. Hegemann, N. De Geyter, R. Morent, K. (Ken) Ostrikov, Plasma-controlled surface wettability: Recent advances and future applications, Int. Mater. Rev. 68 (2023) 82–119, https://doi.org/10.1080/09506608.2022.2047420.
[43] E. Bülbül, D. Hegemann, T. Geue, M. Heuberger, How the dynamics of subsurface hydration regulates protein-surface interactions, Colloids Surf. B Biointerfaces 190 (2020) 110908, https://doi.org/10.1016/j.colsurfb.2020.110908.
[44] E. Bülbül, D. Hegemann, K. Ataka, S. Lehner, J. Heberle, M. Heuberger, Confined hydration in nanometer-graded plasma polymer films: Insights from surface-enhanced infrared absorption spectroscopy, Surf. Interfaces 23 (2021) 100922, https://doi.org/10.1016/j.surfin.2020.100922.